UNIVERSITY OF MICHIGAN — Michigan Engineering

NERS/BIOE 481

Lecture 06
Radioisotope Image Formation

Michael Flynn, Adjunct Prof
Nuclear Engr & Rad. Science
mikef@umich.edu
mikef@rad.hfh.edu

Henry Ford Health System
RADIOLOGY RESEARCH

IV.G - General Model – radioisotope imaging

Radioisotope imaging differs from x-ray imaging only with respect to the source of radiation and the manner in which radiation reaches the detector

DETECTION DISPLAY

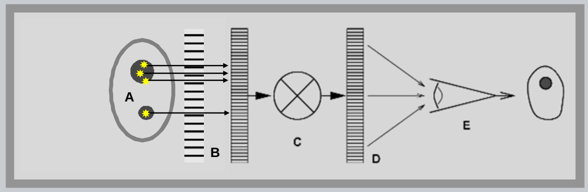

Pharmaceuticals tagged with radioisotopes accumulate in target regions. The detector records the radioactivity distribution by using a multi-hole collimator.

IV.G.1 – Radioisotope Imaging – Collimator designs (11 Charts)

G) Radioisotope Imaging - Primary Signal

1) Collimator designs
2) Parallel hole Collimator - Resolution
3) Parallel hole Collimator - Efficiency
4) Electronic Collimation (Compton Cam.)
5) Coded Aperture Collimation

IV.G.1 – Activity Projection & self absorption

The radioisotope imaging signal is proportional to the line integral of the concentration of radioactive material along a projection vector.

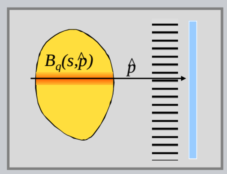

$$S \propto \int_0^S f_a B_q(s,\hat{p})ds$$

B_q : Activity in Becquerel, disintegrations/sec

Due to self absorption, the activity deep in the object is attenuated more that that near the surface. Additionally, the response may be modified by the collimators depth dependence (red region).

$$S = k\int_0^{s_p} f_a B_q(s,\hat{p})G(s)e^{-\mu(s_p-s)}ds$$

NOTE: Since this is not a line integral, it is not amenable to inverse radon transform solutions.

IV.G.1 – Uptake probe collimators

Radioactive iodine uptake tests are used to evaluate thyroid function.

- The patient ingests radioactive Iodine (I-123 or I-131) capsules
- After a delay of 6 to 24 hours, a gamma probe is placed over the thyroid gland to assess the amount of Iodine in the thyroid gland.
- The probe signal is related to the signal from a neck phantom to determine the percent uptake of iodine.

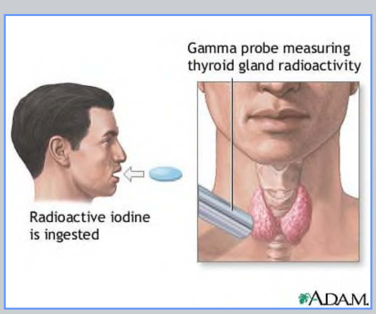

IV.G.1 – Uptake probe collimators

Prior to administration the capsule is placed in a phantom and a measurement made at a measured distance. After correction for decay, the patient measurement is related to the phantom measurement.

Neck Phantom
ORINS, ca 1959

Biodex Atomlab 950, 2008

Picker uptake probe, Circa 1965

IV.G.1 – Uptake probe collimators

The collimator on an uptake probe is a single large tube placed in front of a single crytal gamma ray detector.

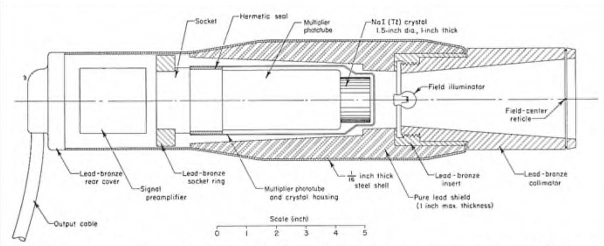

FIG. 6. Schematic of collimator and crystal assembly. The light bulb illuminates an area corresponding to the field of vision. (Courtesy of Picker Nuclear.)

IV.G.1 – Multi-hole probe collimators

By constructing the probe collimation with multiple holes pointing towards a common spot, the response region is greatly reduced.

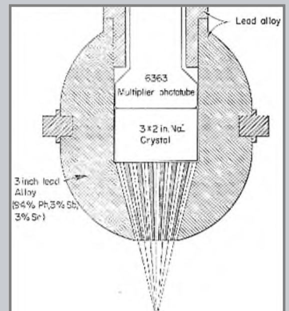

From Hine 1967

IV.G.1 – Multi-hole probe collimators

By scanning the multi-hole collimated detector in a rectilinear pattern, an image was of radioisotope distribution can be recorded. These systems were used extensively from 1965-1975.

CAP Brain Phantom Scan

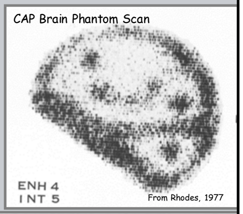

From Rhodes, 1977

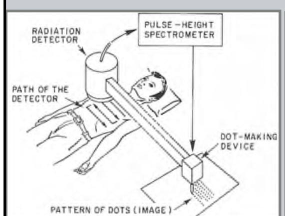

From Sorenson, vol 1

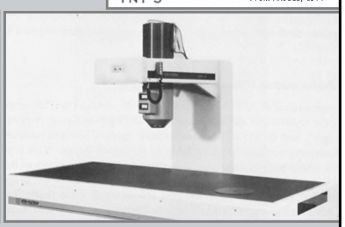

Ohio-Nuclear rectilinear scanner, circa 1970

IV.G.1 – Multi-hole probe collimators

The diameter, length, shape, and direction of the holes influences the response of the multi-hole probe collimator.

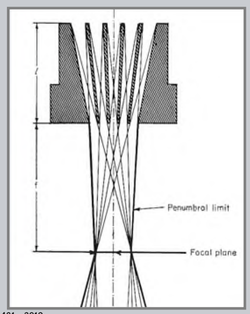

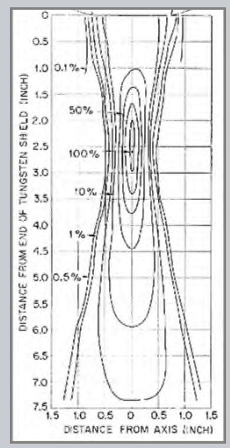

IV.G.1 – Pinhole imaging collimators

Right: the resolution depends on the size of the pinhole.

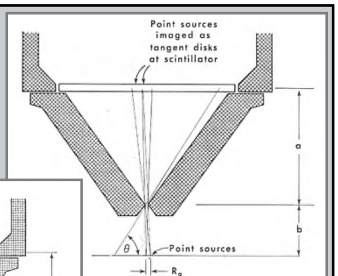

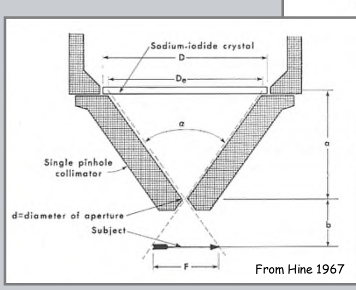

From Hine 1967

Left: magnification increases in relation to the distance of the object from the pinhole.

IV.G.1 – Multi-hole imaging collimators

"However, for large gamma-ray emitting subjects, such as the brain or liver, collimators with large numbers of parallel holes give the best combination of efficiency and resolution."

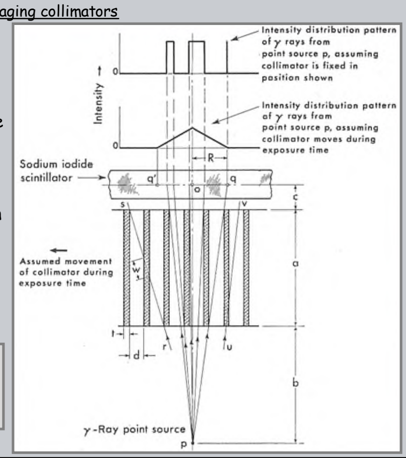

Anger HO,
Scintillation Camera with Multichannel Collimators;
Journal of Nuclear Medicine,
vol 5, pg 515, 1964

IV.G.1 – Multi-hole imaging collimators

Collimator hole shapes.

- Hexagonal
- Square
- Circular
- Triangular

Creativ Microtech
Micro collimator made by
X-ray lithography

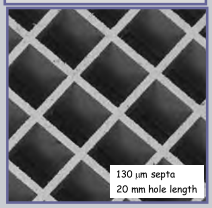

Beck RN , Collimator Design .., IEEE TNS, 32-1, 1985

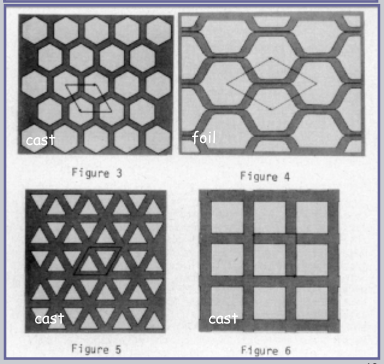

IV.G.1 – Multi-hole imaging collimators

- Most collimators are now made of corrugated lead foil.
- The surface of a collimator core looks much like a honey-comb.
- The delicate structure of the core is protected by a laminate cover.

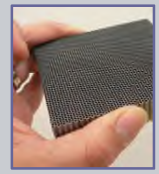

Collimator fabrication using formed lead foils (Nuclear Fields)

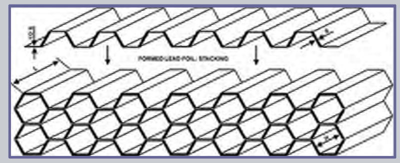

http://www.nuclearfields.com/

IV.G.2 – Radioisotope Imaging – Collimator resolution (4 Charts)

G) Radioisotope Imaging - Primary Signal

1) Collimator designs
2) Parallel hole Collimator - Resolution
3) Parallel hole Collimator - efficiency
4) Electronic Collimation (Compton Cam.)
5) Coded Aperture Collimation

IV.G.2 – collimator spatial response

- The collimator spatial response of a thin slab, parallel hole collimator may be derived by considering the 2D fluence rate at the surface of the detector (i.e. behind the collimator) in relation to the fluence rate incident on the collimator;

$$g(x,y) = \phi_D(x,y) \Big/ \phi_C(x,y)$$

- For a point source of radioactivity, the fluence rate at the near surface of the collimator is given by;

$$\phi_C(x,y) = \frac{f_\gamma B_q}{4\pi D_{sc}^2}$$

$$x \ll D_{sc}, \quad y \ll D_{sc}$$

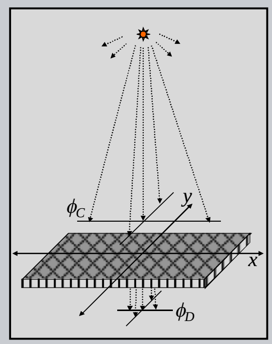

IV.G.2 – collimator spatial response

- Only gamma rays traveling in a direction that pass through an open hole in the collimator will pass to the detector. For perfect absorption in the septa the response function along the x or y axis may be deduced trigonometrically;

$$g(x,0) = \left(1 - \frac{|x|}{R_C}\right) \quad x \le R_C$$

$$R_C = D_{sc}\frac{d}{l}$$

- Note that the *FWHM* of *g(x,0)* is just equal to R_C. The value of R_C is often written in terms of an effective length that accounts for septal transmission.

$$R_C = (D_{SC} + l_e)\frac{d}{l_e}$$

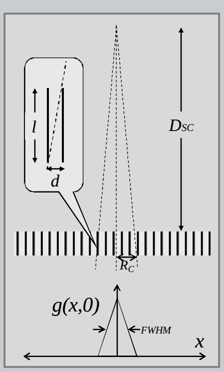

IV.G.2 – collimator spatial response

For a 2D grid with square holes, the fluence rate reduction is deduced by multiplying the response in the x direction by that in the y direction. The isocontours of the response are approximately circular with

$$FWHM = R_C$$

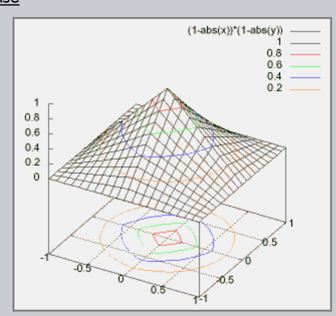

$$g(x,y) = g(x,0)\,g(0,y) = \left(1 - \frac{|x|}{R_C}\right)\left(1 - \frac{|y|}{R_C}\right) \quad ; \quad x, y \le R_C$$

- For nuclear medicine collimators, resolution always degrades with distance from the surface.
- The slope of this degradation depends on the aspect ratio, d/l, of the collimator holes.

$$FWHM = (D_{sc} + l)\frac{d}{l}$$

$$= D_{sd}\frac{d}{l}$$

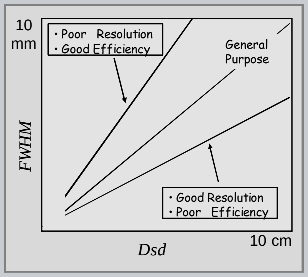

We see in the next section that collimators with low d/l and good resolution have poor efficiency.

G) Radioisotope Imaging - Primary Signal
1) Collimator designs
2) Parallel hole Collimator - Resolution
3) Parallel hole Collimator - Efficiency
4) Electronic Collimation (Compton Cam.)
5) Coded Aperture Collimation

- The collimator efficiency, G, is defined as the total number of photons/sec passing through the collimator and striking the detector in relation to the radioisotope photon emission rate in photons/sec (Bq).
- The count rate at various positions on the detector is;

$$\phi_D(x,y) = g(x,y)\frac{f_\gamma B_q}{4\pi D_{sd}^2}$$

- The collimator efficiency is then;

$$G = \frac{\iint \varphi_D(x,y)\,dxdy}{f_\gamma B_q} = \frac{\iint g(x,y)\,dxdy}{4\pi D_{sd}^2}$$

Note: the efficiency is NOT the detector count rate observed with and without the collimator in place. By convention, it is defined relative to the source strength.

For a square hole collimator with thin but fully absorptive septa, we can evaluate the integral over the fluence rate function to get G.

Using transformed variables, the integral is evaluated using the symmetric shape of ϕ_D to adjust the range of the integrals;

$$x' = \frac{x}{R_C}\,,\quad \frac{dx'}{dx} = \frac{1}{R_C}$$

$$y' = \frac{y}{R_C}\,,\quad \frac{dy'}{dy} = \frac{1}{R_C}$$

$$R_c = D_{sd}\frac{d}{l}$$

see s18 & s19

$$G = \frac{\iint g(x,y)\,dxdy}{4\pi D_{sd}^2}$$

$$= \frac{R_C^2}{4\pi D_{sd}^2}\int_{-1}^{1}\int_{-1}^{1}(1-|x'|)(1-|y'|)dx'dy'$$

$$= \frac{1}{4\pi}\left(\frac{d}{l}\right)^2 4\int_0^1(1-x')dx'\int_0^1(1-y')dy'$$

$$= \frac{1}{4\pi}\left(\frac{d}{l}\right)^2 4\left(\frac{1}{2}\right)\left(\frac{1}{2}\right) = \frac{1}{4\pi}\left(\frac{d}{l}\right)^2$$

Sorenson writes the expression for collimator efficiency as;

$$G = K^2\left(\frac{d}{l_e}\right)^2\left(\frac{d}{d+t}\right)^2$$

An effective length, l_e, is used and a term is included to account for the finite width, t, of the collimator septa (Sorenson equation 16-7).

For K, he gives,

Square Holes	$K = \sim 0.28$
Hexagonal Holes	$K = \sim 0.26$
Round Holes	$K = \sim 0.24$

The value for square holes is consistent with the value we have just derived,

$K^2 = 1/(4\pi)$, $K = 0.282$

Low energy collimators
Sorenson, Table 16.2

type	G	Rc @10cm
High Resolution	1.8×10^{-4}	7.4 mm
General Purpose	2.7×10^{-4}	9.1 mm
High Sensitivity	5.7×10^{-4}	13.4 mm

Note that the efficiency is independent of distance from the collimator and dependent on aspect ratio, d/l, squared.

G => photons transmitted / photons emitted

- The collimator efficiency for a radioisotope source distributed uniformly on a plane sheet is of interest to consider.
- If Bq Becquerel's of activity is distributed over an area A and the emission is in all directions (4π sr), the source emittance will be,

$$\frac{1}{4\pi}\frac{f_\gamma B_q}{A}\,,\quad \#/\sec/sr/cm^2$$

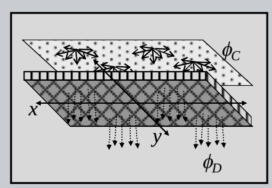

- When the distance from the collimator to the plane source is small relative to the length and width of the collimator, then the irradiance of the surface is equal to the emittance of the source.

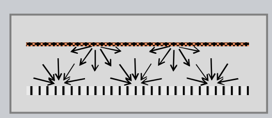

$$\phi_C = \frac{1}{4\pi}\frac{f_\gamma B_q}{A}\,,\quad \#/\sec/sr/cm^2$$

- The collimator efficiency for a radioisotope source distributed uniformly on a plane sheet is given by that portion of the emission rate in *#/cm2/sec* that passes through the collimator divided by the source strength per unit area in *#/cm2/sec*.

$$G = \frac{\frac{1}{4\pi}\left(f_\gamma B_q / A \right)\Omega_C}{f_\gamma B_q / A} = \frac{1}{4\pi}\Omega_C$$

Where the term Ω_C is the solid angle for which the collimator holes can transmit radiation.

- Evaluation of the collimator efficiency for a plane source thus involves determining the transmittance solid angle using an integration over differential solid angle elements.

EQ FROM L03
$d\Omega = \sin(\phi)\, d\phi\, d\theta$

- For a square hole collimator we can evaluate Ω_C by considering a square tube in the x direction.
- $Sin(\phi)$ is therefore 1.0 and $d\Omega = d\theta d\phi$.
- Thus;

$$\Omega_C = \int_{-d/2l}^{+d/2l}\int_{-d/2l}^{+d/2l} d\theta d\phi = \left(\frac{d}{l}\right)^2$$

$$G = \frac{1}{4\pi}\left(\frac{d}{l}\right)^2$$

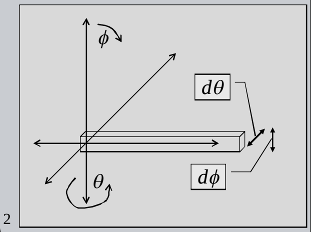

The efficiency for a plane source is thus, as might be expected, the same as for a point source.

EQ FROM L03
$d\Omega = \sin(\phi)\, d\phi\, d\theta$

- For a round hole collimator we can evaluate Ω_C by considering a tube in the z direction.

$$\Omega_C = \int_0^{2\pi} d\theta \int_0^{d/2l} \sin\phi d\phi$$

Where d is now the diameter of the tube.

- Since $sin\phi$ is approximately ϕ for small angles, we can write;

$$\Omega_C = 2\pi\int_0^{d/2l}\phi d\phi$$

$$= 2\pi\left[\frac{1}{2}\left(\frac{1}{2}\frac{d}{l}\right)^2\right] = \frac{\pi}{4}\left(\frac{d}{l}\right)^2$$

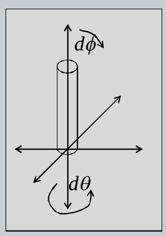

$$G = \frac{\Omega_C}{4\pi} = \left(\frac{1}{4}\right)^2\left(\frac{d}{l}\right)^2$$

The value of $K = 0.25$ is consistent with Sorenson.

G) Radioisotope Imaging - Primary Signal

1) Collimator designs
2) Parallel hole Collimator - Resolution
3) Parallel hole Collimator - efficiency
4) Electronic Collimation (Compton Cam.)
5) Coded Aperture Collimation

- Conventional geometric collimators have very low efficiency for the imaging resolution typically required.
- An advanced method for collimation uses two detectors to estimate the source position without a physical collimator.

- A vector from the source plane is calculated from the interaction positions in both A and B .

$(u,v)_A$, $(u,v)_B$

- The energies deposited in A & B are used to deduce the cone angle, θ.

E_A ,E_B

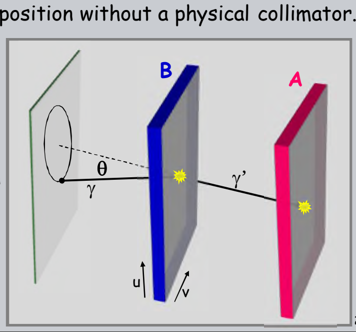

For gamma rays that undergo a Compton scattering interaction in detector B and full energy absorption in detector A, the angle of scattering can be deduced from the Compton scattering equation described in lecture 2.

From L02

$$\frac{1}{E'_\gamma} - \frac{1}{E_\gamma} = \frac{1}{E_\gamma}\alpha(1-\cos\theta)$$

$$\alpha = \frac{E_\gamma}{m_o c^2}$$

$$m_o c^2 = 511(keV)$$

For detection events observed in detector A at time t_A and in detector B at time t_B;

If: $\longrightarrow$ $E_A + E_B = E_\gamma$

and $t_A = t_B$

Then: $\rightarrow$ $E'_\gamma = E_A$

$$\rightarrow \cos\theta = 1 - m_o c^2\left(\frac{1}{E'_\gamma} - \frac{1}{E_\gamma}\right)$$

IV.G.4 – Electronic Collimation

- Reconstruction is done by observing the intersection of the ellipses in the source plane observed from many events.

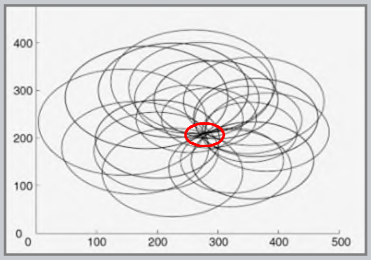

Sample reconstructions of a point source (99mTc) in air shown in the image plane as intersecting conics.

- Polarization and Doppler broadening interaction effects limit the resolution of the reconstructed image.

Chelikani et.al. Phys. Med. Biol. 49 (2004)

IV.G.4 – Compton Cameras

- A Compton camera was first suggested by Everett in 1977 and first constructed by Singh (1983).
- In 1992, Engdahl patented geometries with improved sensitivity.

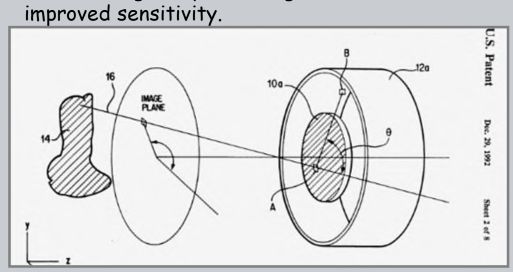

- Everett et.al. : Gamma-radiation .. system based on the Compton effect, 1977 Proc. Inst. Electr. Eng.
- Singh et.al.: An electronically collimated gamma camera ..., 1983 Med. Phys.
- Engdahl, Compton Scatter Camera, US Patent 5,175,434, 19-DEC-1992

IV.G.4 – Compton Cameras

- A Compton camera with a ring detector, C-Sprint, was developed and studied at the University of Michigan in the 1990s.
- While a continuing subject of research, Compton camera devices have not achieved common use for medical studies.

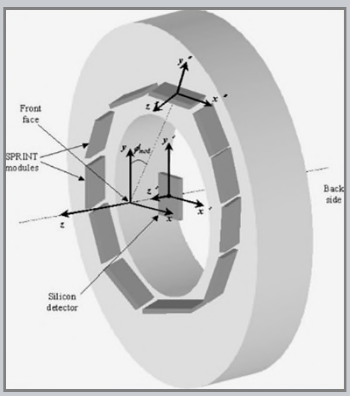

- LeBlanc et.al.: C-SPRINT: a prototype Compton camera system for low energy gamma ray imaging, 1998 IEEE Trans. Nucl. Sci.

IV.G.4 – Compton Cameras in Astronomy

The NASA Compton Gamma Ray Observatory (CGRO) operated a low orbit Compton Telescope, COMPTEL, from 1991-2000.

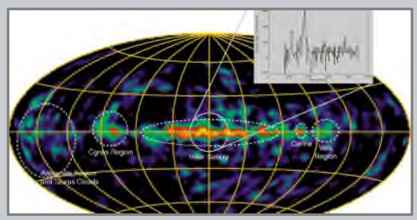

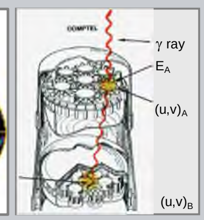

This COMPTEL map shows the Milky Way at an energy of 1.8 MeV which is the characteristic energy of 26Al. 26Al is thought to originate from nucleosynthesis in supernovae. Because gamma rays at these energies traverse the interstellar medium with negligible absorption, COMPTEL maps at 1.8 MeV provide an efficient way to trace sites of nucleosynthesis in the Galaxy.

http://heasarc.gsfc.nasa.gov/docs/cgro/index.html

IV.G.4 – Compton Cameras for security

University of Michigan
http://czt-lab.engin.umich.edu/index.html

Compton cameras have been of recent interest for the detection of unknown isotope sources.

A 3D CdZnTe detector can provide 3D position information as well as energy information of each individual interaction when a gamma ray is scattered or absorbed in the detector. This unique feature provides the 3D CdZnTe detector the capability to do Compton imaging with a single detector.

Xu, He, Lehner, Zhang, SPIE 2004

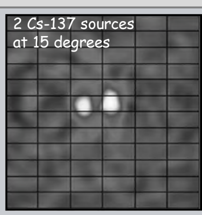

D.Xu, Z. He, NIM-A 574 (2007) 98-109

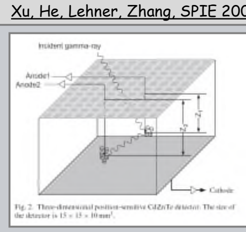

D.Xu, Z. He, NIM-A 574 (2007) 98-109

IV.G.4 – Compton Cameras for security

H3D
www.h3dgamma.com

Polaris-H, 3D CdZnTe Gamma Ray Imaging System

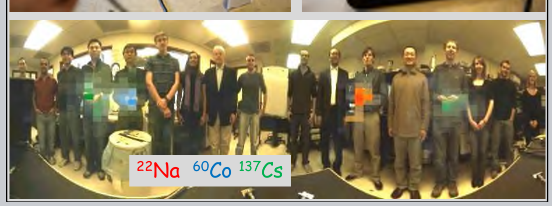

IV.G.5 – Radioisotope Imaging – Coded Aperture Collimation (10 Charts)

G) Radioisotope Imaging - Primary Signal
1) Collimator designs
2) Parallel hole Collimator - Resolution
3) Parallel hole Collimator - efficiency
4) Electronic Collimation (Compton Cam.)
5) Coded Aperture Collimation

IV.G.5 – time coded apertures

- Pin-hole collimators provide very high resolution for small regions of interest.

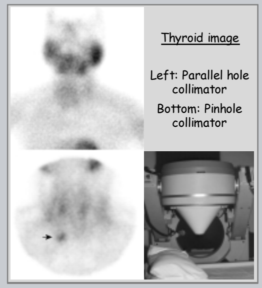

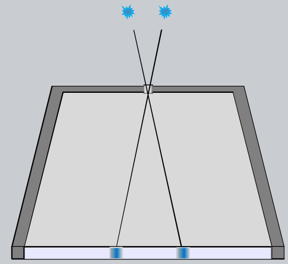

- However, very poor sensitivity limits their use to certain special applications.

IV.G.5 – time coded apertures

Multiple pin-holes improve sensitivity but produce an image with a confusing combination of signals.

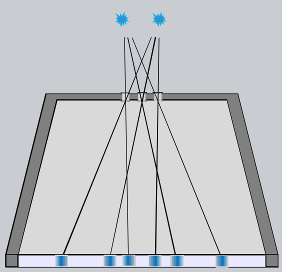

NOTE: A system with seven pin-holes with each exposing a different area of the gamma camera was used briefly until replaced with rotating cameras.
VOGEL RA, KIRCH D, LEFREE MT, et al: A new method of multiplanar emission tomography using a seven pinhole collimator and an Anger scintillation camera.
J Nucl Med 19:648-654, 1978

IV.G.5 – time coded apertures

Time coded multiple apertures
- A sequence of images is acquired over time.
- Each pin-hole is open or closed based on a unique time code.
- The temporal signal at each detector position is analyzed to obtain the image associated with each pin-hole.
- Either temporal correlation of the signal to each aperture code or statistical methods may be used.

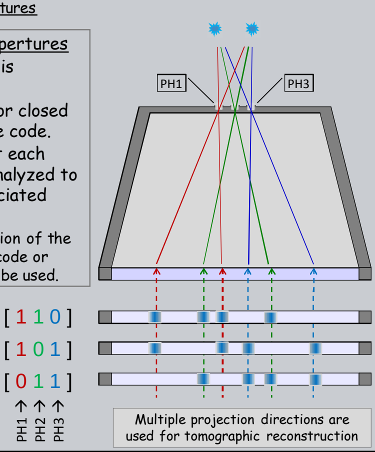

Multiple projection directions are used for tomographic reconstruction

IV.G.5 – time coded apertures

- Several time coded aperture systems were investigated for medical isotope imaging.
- While useful for distributed point sources, they performed poorly for the distributed sources in human subjects.

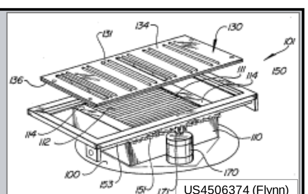

Hybrid Collimator: Neumann 1986 CWRU thesis.

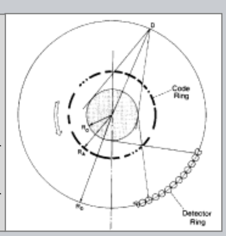

Coded Aperture Ring: Knoll, Rogers, Koral, Stamos, Clinthorn 1984.

Coded Aperture Cam: Koral, Rogers, Knoll 1975.

IV.G.5 – spatially coded apertures

- The spatial position of apertures may also be coded such that an image may be deduce from a single acquisition as opposed to a temporal sequence.
- The source distribution is obtained by correlation of the image signals with the aperture pattern.

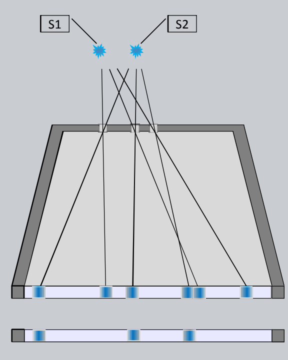

Some of the spatial coding patterns that have been used include;

- Fresnel zone plate
- Optimized random patterns
- Uniform Redundant Array
- Modified Uniformly Redundant Array

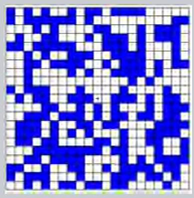

random mask

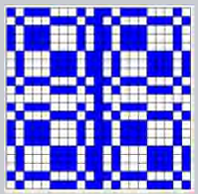

Modified Uniformly Redundant Array

Sonal Joshi, UofM Thesis, 2014

H3D

www.h3dgamma.com

Coded apertures used with the Polaris 3D CZT detector are used for energies less that 250 keV where Compton scatter imaging is less efficient.

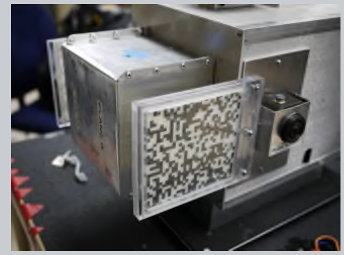

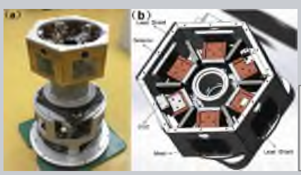

Sun S, Zhang Z, Shuai L, et. al.
".. Panorama coded-aperture camera..
Radiation Measurements, v77, 2015

- 19x19 CsI array
- Positions Sens. PMT
- rank 19 MURA apertures

"A panorama coded-aperture gamma camera optimized for use in complex nuclear environment has been developed and evaluated with an angular resolution of 3.5º."

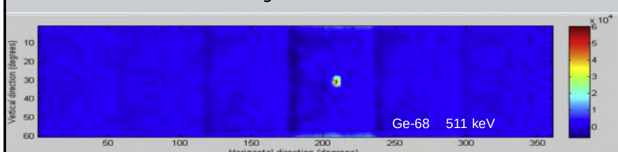

- Satellite coded aperture x-ray imaging telescopes are used for astronomy research.
- The SWIFT satellite, launched in 2004, includes the Burst Alert Telescope (BAT) which records in the 15-150 keV energy range.

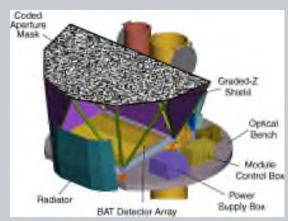

SWIFT BAT Design

Energy Range	15-150 keV
Energy Resolution	~7 keV
Aperture Coded mask	random pattern, 50% open
Detecting Area	5240 cm2
Detector Material	CdZnTe (CZT)
Detector Operation	Photon counting
Detector Elements	256 Modules of 128 elements/Module
Detector Element Size	4.00 x 4.00 x 2.00 mm3
Coded Mask Cell Size	5.00 x 5.00 x 1.00 mm3 Pb tiles
Instrument Dimensions	2.4m x 1.2m x 1.2 m

"The BAT coded aperture is composed of ~52,000 lead tiles located 1 meter above the CZT detector plane. The Pb tiles are 5.00 mm square and 1.0 mm thick. The tiles are mounted on a low-mass, 5-cm thick composite honeycomb panel. The pattern is completely random with a 50% open 50% closed filling factor."

Barthelmy et.al., SPIE v5165, 2004

"It is not technologically possible to produce an image in the gamma-ray band-pass using traditional focusing optics.
Hence, the only way to formulate an image is to use the coded-aperture method."

H) Effects of Scattered Radiation

1) Emission imaging
2) Contrast Reduction
3) Scatter in Radiography

- Emission imaging systems using geometric collimators detect both primary and scattered radiation.
- For scattered radiation, there is no way to determine where the radionuclide is located.

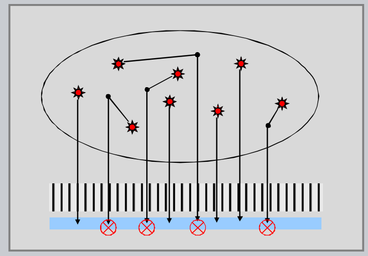

Since the energy of scattered radiation is less than that of the primary radiation, the energy of the detected gamma ray can be used to discriminate against scattered radiation

$$\frac{1}{E_s} - \frac{1}{E_o} = \frac{1}{511}(1-\cos\theta)\ ,\ E\ in\ keV$$

- The spectrum of radiation energies reaching the detector has a large spike at $E = Eo$ and a distribution of lesser energies coming from scattered radiation.
- For ΔE close to Eo (green) the scattered angle is small.
- ΔE is largest for radiation scattered at 180 degrees.

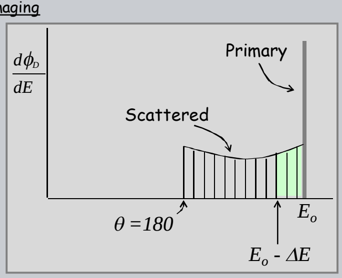

$$\frac{1}{E_o - \Delta E} - \frac{1}{E_o} = \frac{1}{511}(1-\cos\theta)$$

$$\frac{1}{1-\Delta E/E_o} - 1 = \frac{E_o}{511}(1-\cos\theta)$$

For $\Delta E << E_o$

$$\frac{\Delta E}{E_o} \cong \frac{E_o}{511}(1-\cos\theta)$$

$$\frac{\Delta E_{max}}{E_o} \cong \frac{E_o}{255}$$

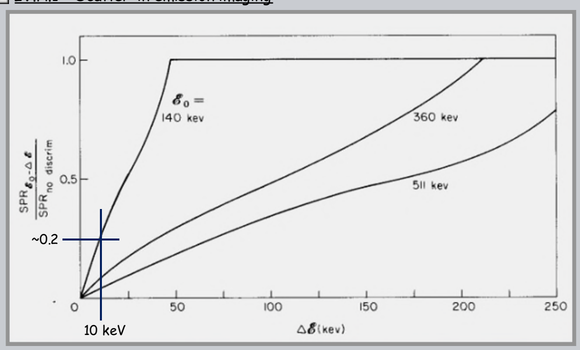

Using a single scatter analytic solution, Barrett illustrates the Scatter to Primary ratio (SPR) achieved with energy discrimination relative to that without. (Barrett & Swindell, Chpt 11, Figure 11.10)

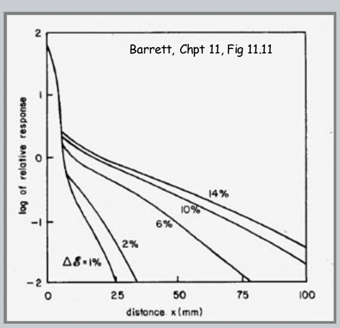

- The blur is shown for a 140 keV line source
- The line spread function (LSF) has a 3mm width for the primary radiation.
- Scatter adds a broad tail dependant on energy discrimination.

The broad LSF tail with low amplitude does not effect the detail in an image. However, it will add a diffuse signal which effects contrast.

H) Effects of Scattered Radiation

1) Emission imaging
2) Contrast Reduction
3) Scatter in Radiography

IV.H.2 - Fog and contrast reduction

Scattered radiation causes contrast reduction in radiation images in the same manner as which fog reduces contrast for a visible scene.

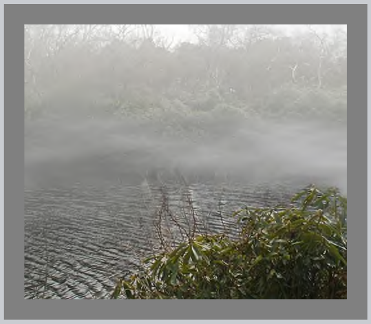

IV.H.2 - Contrast reduction & S/P

- Consider a radiation image with constant primary signal P.
- The primary signal is perturbed by a small object producing contrast of ΔP. The relative contrast without scattered radiation is thus;

  $C_{r:wo} = \Delta P/P$

- We now add the effects of scattered radiation as a constant signal of S. The relative contrast with scatter will be;

  $C_{r:ws} = \Delta P/(P+S)$

- The contrast reduction caused by scatter is thus related to the scatter to primary ratio.

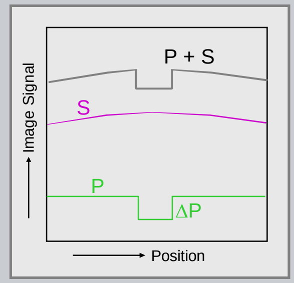

$$\frac{C_{r:ws}}{C_{r:wo}} = \frac{P}{P+S} = \frac{1}{\left(1+\dfrac{S}{P}\right)}$$

IV.H.2 - Scatter and the PSF

- The Point Spread Function, PSF, describes the response of the system to a point source.
  - A small drop of a radioisotope.
  - A thin pencil beam of x-rays.
- The primary radiation beam typically produces a narrow, symmetric function.
- The scattered radiation produces a diffuse signal that may extend over the full field of the image.

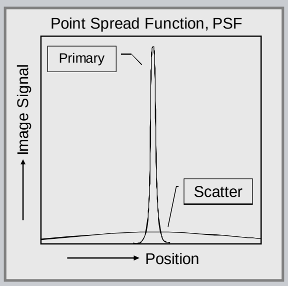

- The total amount of scattered radiation may be similar to the total amount of primary radiation, but the PSF amplitude is very small because it is distributed over a very large area.

IV.H.2 - Scatter and the PSF

- Consider a detector with an array of discrete elements.
- The primary radiation beam incident at element (i',j') with fluence $\phi_P(i',j')$ produces a scattered signal in the other pixels as indicated by the point spread function.

  $PSF(i-i',j-j')\ \phi_P(i',j')$

- The total scatter fluence is obtained by considering the primary fluence at each position.

$$\phi_S(i,j) = \sum_{i'}\sum_{j'} PSF_{(i-i',\,j-j')}\,\phi_P(i',j')$$

- This convolution operation will be covered in the next lecture

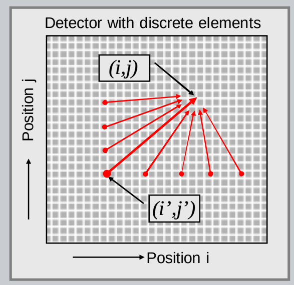

For uniform irradiation of a 100 x 100 array and a constant PSF of 0.001,

$S = 10\ P\ ,\ \ S/P = 10$

IV.H.3 - Effects of Scattered Radiation - radiographic scatter (12 Charts)

H) Effects of Scattered Radiation

1) Emission imaging
2) Contrast Reduction
3) Scatter in Radiography

IV.H.3 - Scattered Radiation

In projection radiography, scattered radiation results from compton scatter events in the volume of the object irradiated. It is most significant for low Z objects examined with high keV x-rays.

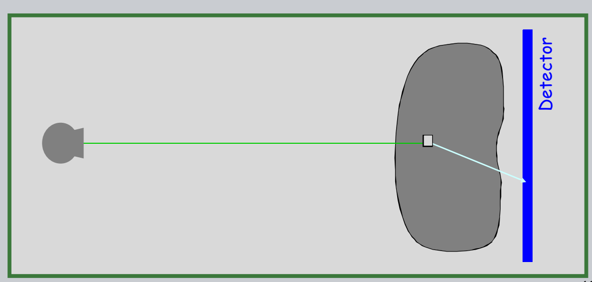

IV.H.3 – Scattered Radiation & grids

- Examination of an object with a large area beam creates a significant scattered signal because of the large volume from which scatter is produced.
- Anti-scatter grids can remove all but the forward scattered component of scatter radiation

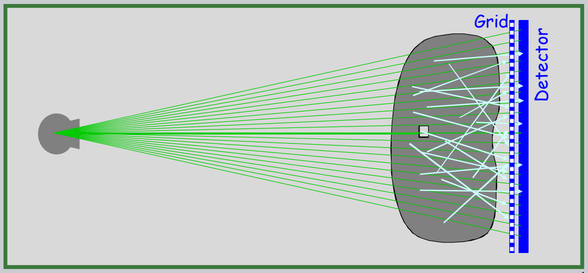

IV.H.3 – Anti-Scattered Grids

- Anti-scatter grids are manufactured by laminating thin sheets of lead alternated with thin sheets of a very low Z and low density material. The composite is then sectioned orthoganal to the planes. The resulting structure has the geometry of a venetian blind.
- For general radiography, the interspace material may be aluminum or composite carbon fiber materials

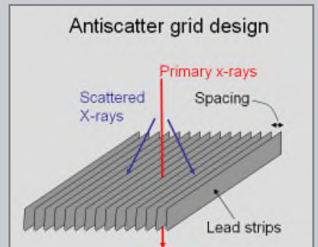

Illustration from SUNY Radiology

IV.H.3 – Anti-Scattered Grid specifications

- Grid Ratio: typically 8 to 12
- Grid Frequency: typically 5.0 – 7.0 lines/mm
- Focused to common Source-Detector distances, 100 or 180 cm

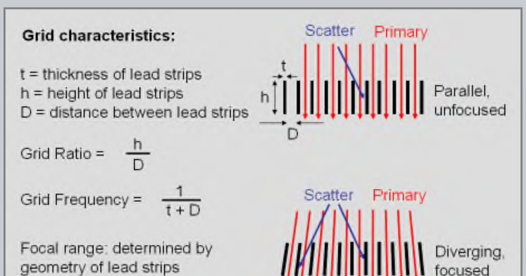

Illustration from SUNY Radiology

IV.H.3 – SPR vs grid ratio

Barrett shows that the open solid angle of a grid is equal to π over the grid ratio, π/G_R .

(Note: Barrett used W and L instead of D and h, see eq 11.114)

$$\Omega_S = \int_0^{2\pi} d\phi \int_{\pi/2+D/2h}^{\pi/2-D/2h} \sin\theta d\theta$$

$$= \frac{\pi}{h/D} = \frac{\pi}{G_R}$$

$$\frac{SPR_w}{SPR_{wo}} = \frac{\pi/G_R}{2\pi} = \frac{1}{2G_R}$$

Scatter-to-Primary Ratios for Various Scatter-Reduction Techniques and X-Ray Tube Voltages[b]

Scatter-reduction technique	X-ray tube voltage 60 kVP	80 kVP	100 kVP	120 kVP
None	5.5	6.6	7.2	7.1
8:1 grid	0.72	1.0	1.2	1.4
12:1 grid	0.48	0.62	0.76	0.87
SMSA	0.16	0.20	0.22	0.22

[a] Taken from Barnes and Brezovich (1979).
[b] Using an 18-cm thick, 30 × 30 cm Lucite phantom.

- For isotropic scattered radiation distributed over 2π, the improvement in scatter to primary ratio is $1/2G_R$.
- In practice, the distribution is more forward peaked and the ratio is larger.

IV.H.3 – Contrast improvement with a grid, 75 kV pelvis radiographs

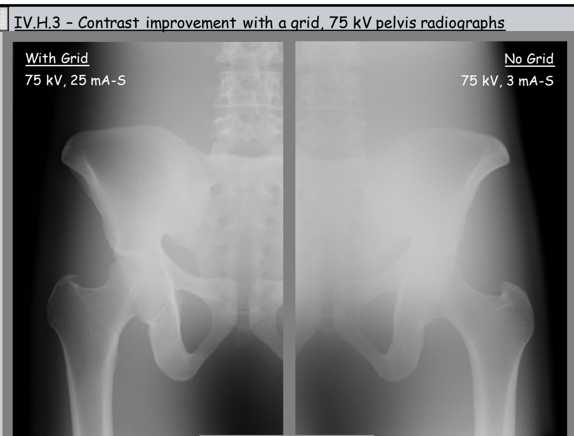

Illustration from SUNY Radiology

IV.H.3 – Scattered Radiation & grids

In general, contrast improvement is always appreciated if the beam is collimated to irradiated only the structures of interest.

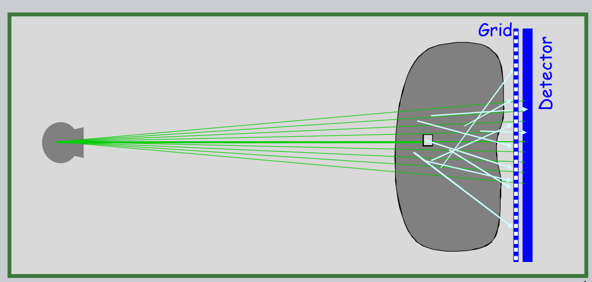

IV.H.3 – Scatter (slot-scan)

- Recently, digital radiography systems have been developed to acquire an image with a scanned fan beam (slot scan).
- Scatter is minimized by the small irradiated volume and by the slot aperture next to the detector.

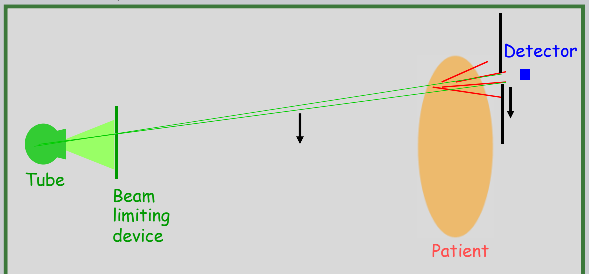

Illustration from Samei, Duke University

IV.H.3 – Scatter Fractions – Chest Radiography

Data from Samei, Duke University

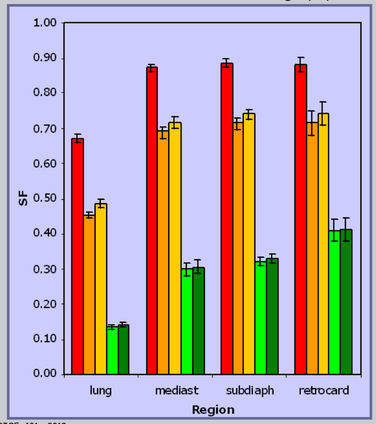

SF = S / (S+P)

S/P = 1/(1/SF-1)

C_{red} =1/(1+S/P)

= (1/SF-1)/(1/SF)

= (1 – SF)

- Full-Field, 120 kVp No Grid
- Full-Field, 120 kVp
- Full-Field, 140 kVp
- Slot-Scan, 117 kVp
- Slot-Scan, 140 kVp

IV.H.3 – Slot scan image quality

Samei, Duke University

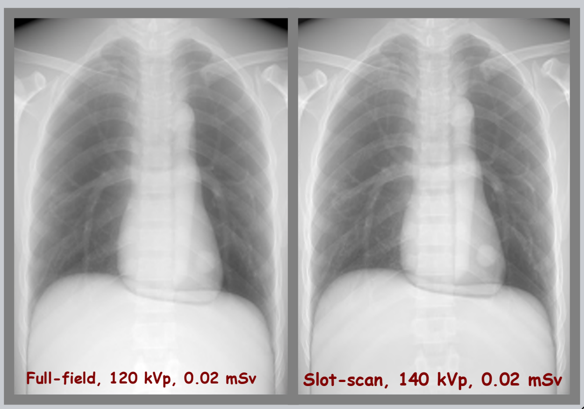

IV.H.3 – Slot scan image quality

Samei, Duke University

Full-field, 120 kVp, 0.02 mSv

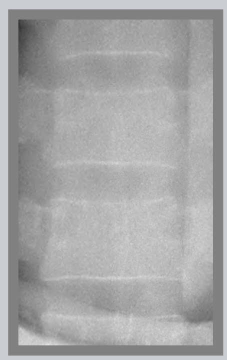

Slot-scan, 140 kVp, 0.02 mSv

IV.H.3 – Slot scan clinical system

- Several manufacturers provide slot-scan medical systems.
- The systems provide large area coverage which has been useful in emergency medicine.
- While images have good contrast, they prone to motion artifacts.

Shimadzu Sonialvision G4

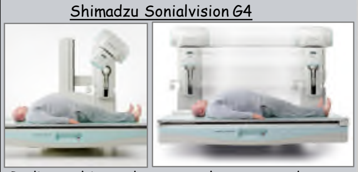

Radiographic mode slot-scan mode